Final Technical Report for USGS National Earthquake Hazards Reduction Program Grants G13AP00024 and G14AP00001

Evaluating the role of injected fluid in triggering the 2011 Oklahoma earthquake sequence: Collaborative Research with the University of Oklahoma and Columbia University

Katie Keranen
Department of Earth and Atmospheric Sciences
Cornell University, Ithaca, NY 14853
Phone: 607-255-6594
Fax: 607-254-4780
keranen@cornell.edu

Heather Savage
Lamont Doherty Earth Observatory of Columbia University
Palisades, NY 10964
Phone: (845) 365-8720
Fax: (845) 365-8150
hsavage@ldeo.columbia.edu

Geoffrey Abers
Department of Earth and Atmospheric Sciences
Cornell University, Ithaca, NY 14853
Phone: 607-255-3879
Fax: 607-254-4780
abers@cornell.edu

Award term: 04/01/2013 through 11/14/2014

Abstract
This grant focused on induced seismicity within the areas of Prague and Jones, OK, and relationships with other induced earthquakes throughout the midwestern US. Research completed under this grant included the location of earthquakes during the Jones, OK earthquake sequence. Additionally, other induced earthquake sequences including Trinidad, CO, and Cogdell, TX were studied, to determine the broader context of activity within which the Prague and Jones earthquakes fall. This work resulted in two publications, both in *Science*, shown in the bibliography below.

Report
Our work focused on induced earthquakes in Oklahoma, as well as other areas of the midwest. The first topic of our work focused on earthquakes in central Oklahoma, particularly near Jones, OK, to help establish the regional context for the seismicity in 2011 near Prague, OK. Prior work had studied the Prague sequence in detail, but not the broader swarm occurring nearby since 2009. This work found that earthquakes migrated through time to the northeast, correlative with fluid pressure migration from large regional wastewater disposal wells (Keranen et al., 2014). Earthquakes in the Jones swarm primarily occurred within the upper 2-5 km, in the Arbuckle Group and within upper basement. Pore pressures modeled using reported monthly disposal rates were sufficient at each earthquake hypocenter to trigger the earthquake.

In the second aspect of our work, we studied whether areas of induced seismicity are susceptible to shaking from remote earthquakes, much like geothermal areas with triggered earthquakes related to high fluid pressure. This work studied the areas of Prague, OK, Trinidad, CO, and Cogdell, TX and three large teleseisms that occurred while the EarthScope Transportable Array was in the Midwestern states (2011 Tohoku earthquake, 2010 Maule earthquake, and 2012 East Indian Ocean earthquake). We found that each of the areas of induced seismicity experienced an uptick in seismicity associated with the shaking of a large teleseism, prior to experiencing its own moderate-sized earthquake. This implies that fluid pressures were high in areas of induced seismicity, and that susceptibility to shaking may be a useful indicator of faults loading up to host a larger earthquake (van der Elst et al., 2013).

Data and methodology for Jones, Oklahoma earthquake catalog
Location of the earthquakes included an initial step to detect earthquakes using a standard STA/LTA (short-term average/long-term average) detector, with an STA window of 0.15 seconds and an LTA window of 2.0 seconds. We applied a 1-30 Hz filter to the data before running the detection algorithm, and required a signal-to-noise ratio of 3.0 to identify each detection. The detections were then associated with earthquakes if a sufficient number of detections were made within 1.5 seconds. These automatically located earthquakes were each inspected by an analyst, and picks were refined. A 1-D velocity model was inverted for using data from earthquakes with at least 15 recorded phases (Keranen et al., 2014). Final earthquake locations for the entire catalog were done in Velest, with a subset of well-recorded earthquakes relocated in HypoDD (Keranen et al., 2014).

Triggering detection: matched filter

In the remote triggering aspect of this study (van der Elst et al., 2013), we used a matched filter as an event detector on continuous waveforms at TA stations to identify un-cataloged earthquakes. In this approach, we started with a set of seismograms from earthquakes known to have occurred in the region of interest, either identified on high-pass filtered seismograms or taken from the ANSS catalog. These seismograms were stacked to produce a template, which was then cross-correlated with the entire continuous recording at a given station. Spikes in the cross-correlation correspond to likely earthquakes in the target location. This allowed us to search quickly and efficiently for earthquakes that may have been too small to register on the multiple seismic stations required to obtain a catalog location. Each detection was visually confirmed.

Data Products

The relocated catalog of Jones earthquakes and the 1D velocity model are published in the supplementary material of Keranen et al., 2014. Waveform data for months of November and December 2011, both the data presented in this report and the entire continuous waveform data, are archived at the USGS in Golden and have been used subsequently (e.g., McNamara et al., 2015). RAMP data are publicly available at the IRIS DMC server, with network code ZQ.

Bibliography of manuscripts produced under this grant

Keranen, K., Weingarten, M., Abers, G., Bekins, B., and Ge. S., (2014), Sharp increase since 2008 induced by massive wastewater injection, *Science*, v. 345, p. 448-451.

van der Elst, N. J., Savage, H. M., Keranen, K. M., and Abers, G. A., Enhanced remote earthquake triggering at fluid-injection sites in the Midwestern U.S., *Science*, 341, p. 164-167, doi; 10.1126/science.1238948.

Sharp increase in central Oklahoma seismicity since 2008 induced by massive wastewater injection

K. M. Keranen *et al.*

Science **345**, 448 (2014);
DOI: 10.1126/science.1255802

Science (print ISSN 0036-8075; online ISSN 1095-9203) is published weekly, except the last week in December, by the American Association for the Advancement of Science, 1200 New York Avenue NW, Washington, DC 20005.

and North Atlantic and indicate the potential for amplification of decadal-scale variability through interbasin resonance (*42*, *43*). Before the 1970s, variability in poleward heat fluxes and storm tracks in the North Pacific and North Atlantic regions were uncorrelated; more recently, highly correlated behavior has emerged (*44*). Our study documents that the development of such teleconnected variability between these regions is a fundamentally important phenomenon associated with rapid warming, suggesting that such properties may be high-priority targets for detailed monitoring in the future.

REFERENCES AND NOTES

1. R. B. Alley *et al.*, *Nature* **362**, 527–529 (1993).
2. J. P. Steffensen *et al.*, *Science* **321**, 680–684 (2008).
3. W. Dansgaard *et al.*, *Nature* **364**, 218–220 (1993).
4. W. S. Broecker, D. M. Peteet, D. Rind, *Nature* **315**, 21–26 (1985).
5. P. U. Clark *et al.*, *Science* **293**, 283–287 (2001).
6. J. F. McManus, R. Francois, J.-M. Gherardi, L. D. Keigwin, S. Brown-Leger, *Nature* **428**, 834–837 (2004).
7. W. S. Broecker, *Paleoceanography* **13**, 119–121 (1998).
8. J. B. Pedro *et al.*, *Clim. Past* **7**, 671–683 (2011).
9. D. C. Lund, A. C. Mix, *Paleoceanography* **13**, 10–19 (1998).
10. O. A. Saenko, A. Schmittner, A. J. Weaver, *J. Clim.* **17**, 2033–2038 (2004).
11. Y. Okazaki *et al.*, *Science* **329**, 200–204 (2010).
12. A. Timmermann, F. Justino, F.-F. Jin, U. Krebs, H. Goosse, *Clim. Dyn.* **23**, 353–370 (2004).
13. Y. M. Okumura, C. Deser, A. Hu, A. Timmermann, S. P. Xie, *J. Clim.* **22**, 1424–1445 (2009).
14. H. Gebhardt *et al.*, *Paleoceanography* **23**, PA4212 (2008).
15. J. P. Kennett, L. B. Ingram, *Nature* **377**, 510–514 (1995).
16. L. Max *et al.*, *Paleoceanography* **27**, PA3213 (2012).
17. A. C. Mix *et al.*, *Geophys. Monogr.* **112**, 127–148 (1999).
18. M. H. Davies *et al.*, *Paleoceanography* **26**, PA2223 (2011).
19. T. M. Lenton *et al.*, *Proc. Natl. Acad. Sci. U.S.A.* **105**, 1786–1793 (2008).
20. V. Dakos *et al.*, *Proc. Natl. Acad. Sci. U.S.A.* **105**, 14308–14312 (2008).
21. V. Dakos, E. H. van Nes, R. Donangelo, H. Fort, M. Scheffer, *Theor. Ecol.* **3**, 163–174 (2010).
22. M. Scheffer *et al.*, *Science* **338**, 344–348 (2012).
23. J. Bakke *et al.*, *Nat. Geosci.* **2**, 202–205 (2009).
24. T. M. Lenton, V. N. Livina, V. Dakos, M. Scheffer, *Clim. Past.* **8**, 1127–1139 (2012).
25. V. N. Livina, T. M. Lenton, *Geophys. Res. Lett.* **34**, L03712 (2007).
26. S. O. Rasmussen *et al.*, *J. Geophys. Res.* **111**, D06102 (2006).
27. B. E. Caissie, J. Brigham-Grette, K. T. Lawrence, T. D. Herbert, M. S. Cook, *Paleoceanography* **25**, PA1206 (2010).
28. J. A. Barron, L. Heusser, T. Herbert, M. Lyle, *Paleoceanography* **18**, PA1020 (2003).
29. C. Waelbroeck *et al.*, *Nature* **412**, 724–727 (2001).
30. E. Bard, F. Rostek, J. L. Turon, S. Gendreau, *Science* **289**, 1321–1324 (2000).
31. W. Broecker, A. E. Putnam, *Quat. Sci. Rev.* **57**, 17–25 (2012).
32. E. Monnin *et al.*, *Earth Planet. Sci. Lett.* **224**, 45–54 (2004).
33. B. Lemieux-Dudon *et al.*, *Quat. Sci. Rev.* **29**, 8–20 (2010).
34. T. M. Cronin *et al.*, *Quat. Sci. Rev.* **29**, 3415–3429 (2010).
35. H. Asahi, K. Takahashi, *Prog. Oceanogr.* **72**, 343–363 (2007).
36. F. Justino, A. Timmermann, U. Merkel, E. P. Souza, *J. Clim.* **18**, 2826–2846 (2005).
37. F. S. R. Pausata, C. Li, J. J. Wettstein, M. Kageyama, K. H. Nisancioglu, *Clim. Past* **7**, 1089–1101 (2011).
38. D. J. Ullman, A. N. LeGrande, A. E. Carlson, F. S. Anslow, J. M. Licciardi, *Clim. Past* **10**, 487–507 (2014).
39. G. Shaffer, J. Bendtsen, *Nature* **367**, 354–357 (1994).
40. M. H. Davies *et al.*, *Earth Planet. Sci. Lett.* **397**, 57–66 (2014).
41. A. J. Weaver, O. A. Saenko, P. U. Clark, J. X. Mitrovica, *Science* **299**, 1709–1713 (2003).
42. L. Wu, Z. Liu, *J. Clim.* **18**, 331–349 (2005).
43. C. Li, L. Wu, Q. Wang, L. Qu, L. Zhang, *Clim. Dyn.* **32**, 753–765 (2009).
44. E. K. M. Chang, *J. Clim.* **17**, 4230–4244 (2004).
45. A. S. Dyke, in *Quaternary Glaciations: Extent and Chronology*, J. Ehlers, P. L. Gibbard, Eds. (Elsevier, Amsterdam, 2004), pp. 373–424.
46. M. Sarnthein, U. Plaufmann, M. Weinelt, *Paleoceanography* **18**, 1047 (2003).

ACKNOWLEDGMENTS

We thank B. Jensen and D. Froese for the tephra analyses; J. Southon for assistance with radiocarbon samples; A. Ross, J. Padman, and J. McKay of the College of Earth, Ocean and Atmospheric Sciences Stable Isotope Lab; and five anonymous reviewers. This work was supported by NSF grants AGS-0602395 (Project PALEOVAR) and OCE-1204204 to A.C.M., and an NSF graduate research fellowship to S.K.P. The data can be found in the supplementary online materials and at the National Oceanic and Atmospheric Administration Paleoclimate Database.

SUPPLEMENTARY MATERIALS

www.sciencemag.org/content/345/6195/444/suppl/DC1
Materials and Methods
Supplementary Text
Figs. S1 to S11
Tables S1 and S2
References (*47*–*66*)

10 February 2014; accepted 24 June 2014
10.1126/science.1252000

INDUCED EARTHQUAKES

Sharp increase in central Oklahoma seismicity since 2008 induced by massive wastewater injection

K. M. Keranen,[1]* M. Weingarten,[2] G. A. Abers,[3]† B. A. Bekins,[4] S. Ge[2]

Unconventional oil and gas production provides a rapidly growing energy source; however, high-production states in the United States, such as Oklahoma, face sharply rising numbers of earthquakes. Subsurface pressure data required to unequivocally link earthquakes to wastewater injection are rarely accessible. Here we use seismicity and hydrogeological models to show that fluid migration from high-rate disposal wells in Oklahoma is potentially responsible for the largest swarm. Earthquake hypocenters occur within disposal formations and upper basement, between 2- and 5-kilometer depth. The modeled fluid pressure perturbation propagates throughout the same depth range and tracks earthquakes to distances of 35 kilometers, with a triggering threshold of ~0.07 megapascals. Although thousands of disposal wells operate aseismically, four of the highest-rate wells are capable of inducing 20% of 2008 to 2013 central U.S. seismicity.

Seismicity in the United States midcontinent surged beginning in 2008 (*1*), predominantly within regions of active unconventional hydrocarbon production (*2*–*6*). In Arkansas, Texas, Ohio, and near Prague, Oklahoma, recent earthquakes have been linked to wastewater injection (*2*–*7*), although alternative interpretations have been proposed (*1*, *8*). Conclusively distinguishing human-induced earthquakes solely on the basis of seismological data remains challenging.

Seismic swarms within Oklahoma dominate the recent seismicity in the central and eastern United States (*9*), contributing 45% of magnitude (M) 3 and larger earthquakes between 2008 and 2013 (*10*). No other state contributed more than 11%. A single swarm, beginning in 2008 near Jones, Oklahoma, accounts for 20% of seismicity in this region (*10*). East of Jones, the damaging 2011 moment magnitude (M_w) 5.7 earthquake near Prague, Oklahoma, was likely induced by wastewater injection (*2*, *8*, *11*, *12*), the highest magnitude to date. These earthquakes are part of a 40-fold increase in seismicity within Oklahoma during 2008 to 2013 as compared to 1976 to 2007 (Fig. 1, inset A) (*10*). Wastewater disposal volumes have also increased rapidly, nearly doubling in central Oklahoma between 2004 and 2008. Many studies of seismicity near disposal wells rely upon statistical relationships between the relative timing of seismicity, disposal well location, and injected water volume to evaluate a possible causal relationship (*3*–*7*, *13*).

Here we focused on the Jones swarm and compared modeled pore pressure from hydrogeological models to the best-constrained earthquake hypocenters (*14*). Using data from local U.S. Geological Survey NetQuake accelerometers, the Earthscope Transportable Array, and a small local seismic network (fig. S1), we generated a catalog of well-located earthquakes between 2010 and 2013. Event-station distances were predominantly less than 10 km (fig. S2D), and all earthquakes were recorded on at least one seismometer within 20 km of the initial hypocenter. To study pore pressure changes at earthquake hypocenters and the apparent migration in seismicity, we developed a three-dimensional hydrogeological model of pore pressure diffusion from injection wells.

The Jones swarm began within 20 km of high-rate wastewater disposal wells, among the highest rate in Oklahoma, between two regions of fluid injection (Fig. 2). The four high-rate wells are southwest of Jones in southeast Oklahoma City (SE OKC) and dispose of ~4 million barrels per month (*15*) (Fig. 3). The target injection depth is 2.2 to 3.5 km into the Cambrian-Ordovician

[1]Department of Earth and Atmospheric Sciences, Cornell University, Ithaca, NY, USA. [2]Department of Geological Sciences, University of Colorado, Boulder, CO, USA. [3]Lamont-Doherty Earth Observatory of Columbia University, Palisades, NY, USA. [4]U.S. Geological Survey, Menlo Park, CA, USA.
***Corresponding author. E-mail: keranen@cornell.edu** †Present address: Department of Earth and Atmospheric Sciences, Cornell University, Ithaca, NY, USA.

Arbuckle Group (fig. S3), a dolomitized carbonate; one disposal well ends near Precambrian basement. The large disposal wells are within dewatering plays (fig. S4). Dewatering production wells produce substantial wastewater volumes with initially up to 200 times as much water per barrel of oil as conventional production wells (*16*, *17*). The rate of wastewater disposal in central Oklahoma has gradually increased since the mid-1990s (fig. S5), but disposal rates jumped after 2004 as high-rate injection wells began operating, including the first of the SE OKC wells in 2005 (Fig. 3) (*15*). Seismic moment release escalated in the Jones swarm in 2009, concurrent with the initial reported application

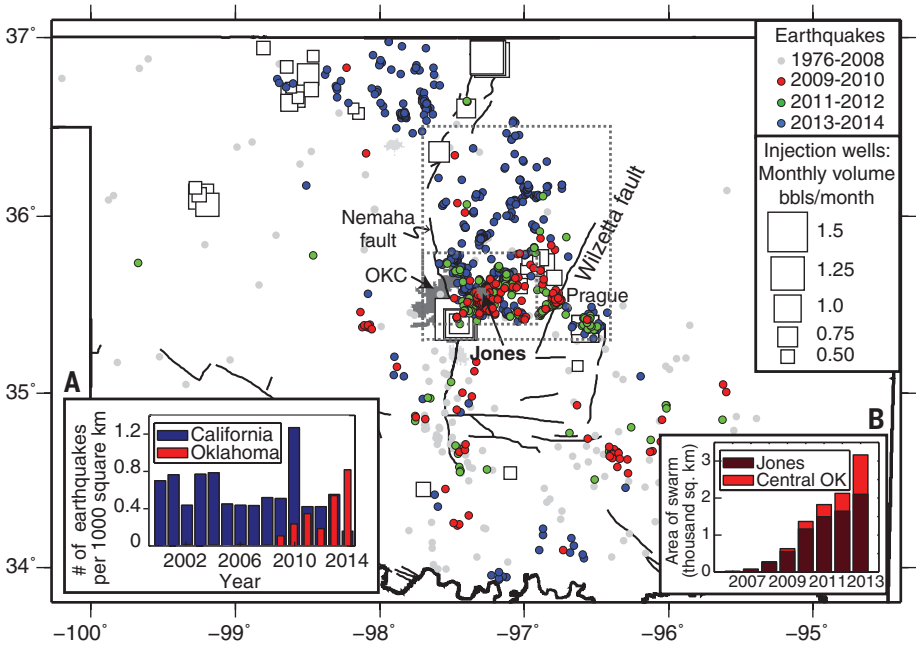

Fig. 1. Earthquakes in Oklahoma between 1976 and 2014. Earthquakes are $M > 1$ from the NEIC catalog (*10*). Black lines are faults (*26*–*28*). Small and large dashed gray boxes outline the areas used for analysis of the Jones swarm and of central Oklahoma, respectively, in inset B. OKC: Oklahoma City. **Inset A:** Comparison of *M*3+ earthquake rate in Oklahoma and California, normalized by area. California is ~2.3 times larger than Oklahoma. 2014 earthquakes are through the first 4 months. **Inset B:** Expanding area of the Jones and the broader central Oklahoma swarms. Regions were divided into 5 km by 5 km grid cells, and any cell with an earthquake was considered part of the swarm. Swarm area per year is inclusive of all prior years.

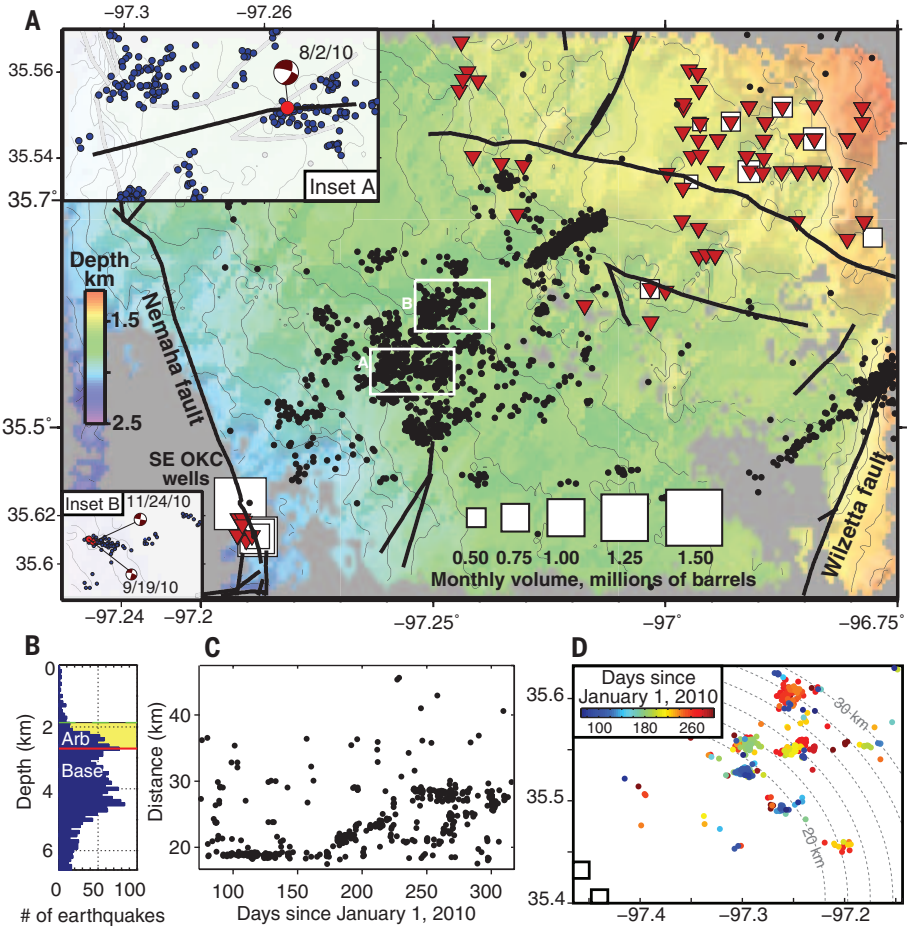

Fig. 2. Earthquake catalog and swarm migration. (**A**) Jones earthquake catalog March 2010 to March 2013 using local stations. Squares are injection wells operating at an average rate ≥ 400,000 barrels per month (*15*, *29*); triangles are high–water production wells. Background color and contours represent depth to the top of the Hunton Group (*15*). The Hunton Group is higher in section than the Arbuckle Group but has more data on formation depth. (**B**) Earthquake depth histogram; earthquakes are dominantly in sediment and upper basement. (**C**) Distance of each March to October 2010 Jones earthquake to the SE OKC disposal wells. The dense region of the swarm increases in distance between days 150 and 250 in 2010. (**D**) Map view of Jones earthquakes during March to October 2010, colored by time. Semicircles are equidistant lines from SE OKC disposal wells. Faults at greater distance from the wells become active at later times. Details of two of these fault planes are shown in insets of Fig. 2A and are discussed in the text.

of positive wellhead pressure at the SE OKC wells (Fig. 3B).

Earthquakes in our catalog primarily nucleated either within the Arbuckle Group or within the upper 2 km of basement, with 22 to 33% above basement (Fig. 2B and fig. S6). Well-constrained earthquake hypocenters from March to October 2010 migrated northeast from the initial swarm centroid near Jones at 0.1 to 0.15 km/day (Fig. 2, C and D), followed by a broad spread in seismicity. Earthquake hypocenters are not diffusely distributed; instead, relocated aftershock sequences of individual earthquakes (*18*) illuminate narrow faults parallel to one plane of calculated focal mechanisms (*19*) (Fig. 2A, insets). An earthquake on 2 August 2010 ruptured a portion of a 7-km-long mapped fault; if the entire fault had ruptured, earthquake scaling laws suggest a maximum magnitude of ~*M*6.0 (*20*). Earthquakes later in 2010 ruptured an unmapped east-southeast– to west-northwest–trending fault, at an oblique angle to the overall northeast-southwest migration direction of the swarm. Although the swarm of seismicity migrates to the northeast parallel to structural dip, the individual faults, as evidenced by earthquake lineations, are not preferentially oriented in this direction.

Our hydrogeological model simulated injection into the Arbuckle Group using reported injection rates at 89 wells within 50 km of the Jones swarm between 1995 and 2012 (*14*). The wells include the four high-rate wells in SE OKC and 85 wells to the northeast of Jones. The model predicts a region of high fluid pressure perturbation spreading radially eastward from the SE OKC wells and a lesser perturbation around the lower-rate wells to the northeast (Fig. 4). The high pore pressure increase occurs within the Arbuckle Group and in the upper 1 to 2 km of the basement in our model; nearly all earthquakes occur within this same depth range (Fig. 2B). The migrating front of the Jones earthquake swarm corresponds closely to the expanding modeled pressure perturbation away from the SE OKC wells, which reaches 25 km from the wells by December 2009 and ~35 km by December 2012. The pore pressure change modeled at each hypocenter indicates a critical threshold of ~0.07 MPa, above which earthquakes are triggered. This threshold is compatible with prior observations that static stress changes of as little as ~0.01 to 0.1 MPa are sufficient to trigger earthquakes when faults are near failure in the ambient stress field (*21*–*23*).

Our results indicate that for modeled diffusivities, ~85% of the pore pressure perturbation is contributed by the four high-rate SE OKC wells. The 85 wells to the northeast contribute ~15% additional pore pressure change at the center of the Jones swarm by the end of 2012 and may contribute to the triggering of earthquakes particularly outside the region affected by the SE OKC wells (fig. S7). The modeled dominance of the SE OKC wells is attributable to their high rate; these wells include one of the largest wells in the state and three closely spaced wells 3.5 km away with a combined monthly volume of ~3 million barrels per month. The only other Oklahoma wells of similar size, in northern Oklahoma (fig. S8), are on the boundary of a second rapidly growing seismic swarm (Fig. 1). The summed rate of this well cluster near SE OKC is higher than previous cases of reported induced seismicity (Fig. 3A), including several times higher than the high-rate disposal wells linked to earthquakes near Dallas–Fort Worth, Texas, and Cleburne, Texas (*5*–*7*). Comprehensive compilations of injection well rates for other high-injection states, including Texas and California, are not yet accessible.

We view the expanding Jones earthquake swarm as a response to regionally increased pore pressure from fluids primarily injected at the SE OKC wells. As the pressure perturbation expanded and encountered faults at various orientations, critically stressed, optimally oriented faults are expected to rupture first (*24*). Additional faults at near-optimal orientations may rupture after further pressure increase (Fig. 4). As fluid pressure continues to

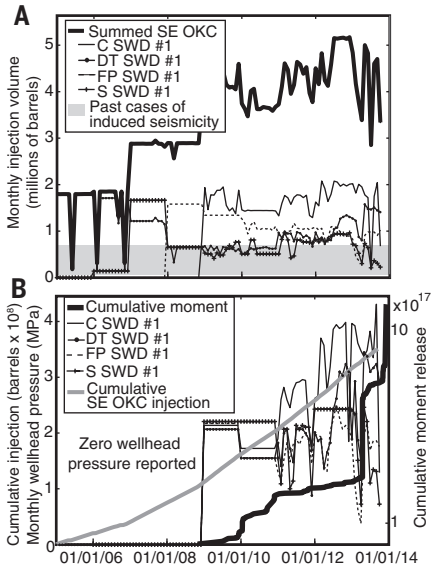

Fig. 3. Fluid injection reported in the four high-rate SE OKC wells. (**A**) Sum and individual monthly injection volumes and (**B**) wellhead pressure and cumulative, summed injected volume (*15*). The DT SWD #1, FP SWD #1, and S SWD #1 wells are in close proximity; the C SWD #1 well is ~3.5 km away. Gray shading denotes injection rates for notable past cases of induced seismicity for reference (table S1). Cumulative seismic moment in (B) is calculated from *M*3+ earthquakes from 2005 to January 2014 (*10*) for earthquakes within the box outlining the Jones swarm in Fig. 1.

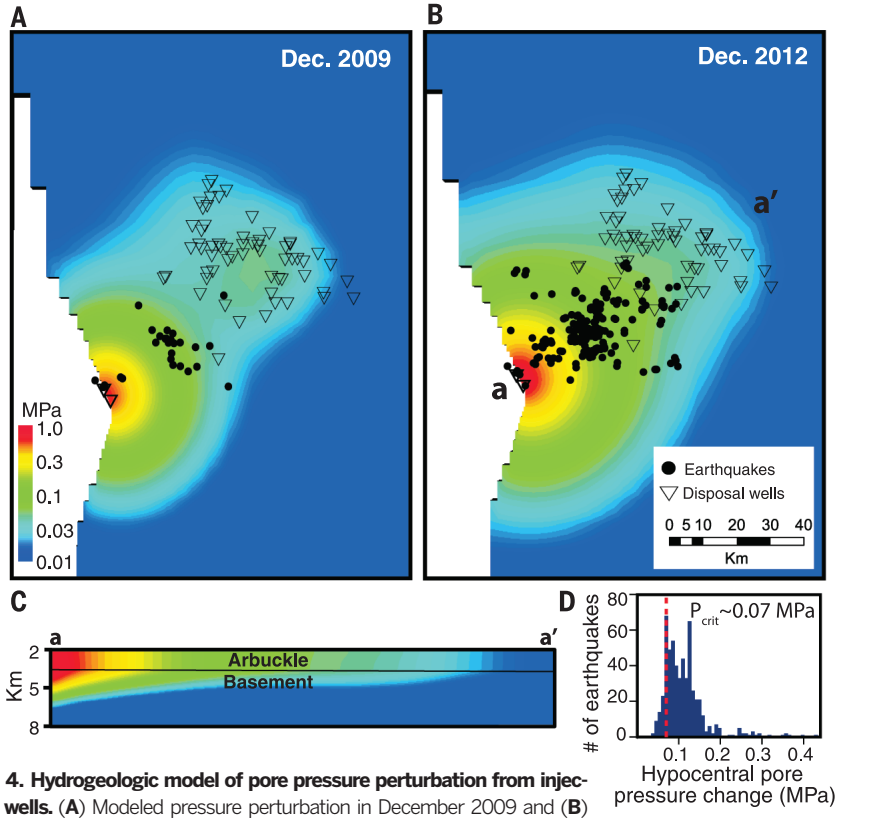

Fig. 4. Hydrogeologic model of pore pressure perturbation from injection wells. (**A**) Modeled pressure perturbation in December 2009 and (**B**) in December 2012 with a hydraulic diffusivity of 2 m^2/s (*14*). The model includes the four high-rate SE OKC wells and 85 wells northeast of the Jones swarm near the West Carney field. The modeled pressure perturbation is dominated by fluid injected at the high-rate SE OKC wells. Earthquakes are plotted from 2008 to 2009 (A) and 2008 to 2012 (B) (*10*). (**C**) Vertical cross section through model results. Pore pressure rises in the Arbuckle Group and uppermost basement. (**D**) Pore pressure increase at the hypocenter of each earthquake in our local catalog. A pore pressure increase of ~0.07 MPa is the modeled triggering threshold. Modeled pore pressure rises throughout much of the swarm area for hydraulic diffusivity between 1 and 4 m^2/s (fig. S7).

propagate away from the wells and disturbs a larger and larger volume, the probability increases that fluid pressure will encounter a larger fault and induce a larger-magnitude earthquake. The absence of earthquakes in regions above the critical pressure threshold may result from either a lack of faults or lack of well-oriented, critically stressed faults. Alternatively, fluid flow may preferentially migrate along bedding structure (Fig. 2A).

Though seven earthquakes were recorded in 2006 to 2009 near the base of the SE OKC wellbores (*10*), the main swarm began ~15 km to the northeast (fig. S9), despite the high modeled pressure perturbation near the wells. Earthquakes in 2009 primarily occurred, within location uncertainty, near injection wells or on the nearest known faults to the northeast of the wells (fig. S9). Focal mechanisms near the swarm onset indicate fault planes at orientations favorable to failure (*19*) (Fig. 2, inset B). Faults subparallel to the north-northwest–south-southeast–trending Nemaha fault would not be well oriented for failure in the regional ~N70E stress regime (*25*) and would require substantially larger pressure increase to fail. Recent earthquakes near the fault may be evidence for continued pressure increase. This 50-km-long segment of the Nemaha fault is capable of hosting a *M*7 earthquake based on earthquake scaling laws (*20*), and the fault zone continues for hundreds of kilometers. The increasing proximity of the earthquake swarm to the Nemaha fault presents a potential hazard for the Oklahoma City metropolitan area.

Our earthquake relocations and pore pressure models indicate that four high-rate disposal wells are capable of increasing pore pressure above the reported triggering threshold (*21*–*23*) throughout the Jones swarm and thus are capable of triggering ~20% of 2008 to 2013 central and eastern U.S. seismicity. Nearly 45% of this region's seismicity, and currently nearly 15 $M > 3$ earthquakes per week, may be linked to disposal of fluids generated during Oklahoma dewatering and after hydraulic fracturing, as recent Oklahoma seismicity dominantly occurs within seismic swarms in the Arbuckle Group, Hunton Group, and Mississippi Lime dewatering plays. The injection-linked seismicity near Jones occurs up to 35 km away from the disposal wells, much further than previously considered in existing criteria for induced seismicity (*13*). Modern, very high-rate injection wells can therefore affect regional seismicity and increase seismic hazard. Regular measurements of reservoir pressure at a range of distances and azimuths from high-rate disposal wells could verify our model and potentially provide early indication of seismic vulnerability.

REFERENCES AND NOTES

1. W. L. Ellsworth, *Science* **341**, 1225942 (2013).
2. K. Keranen, H. Savage, G. Abers, E. Cochran, *Geology* **41**, 699–702 (2013).
3. W.-Y., *J. Geophys. Res.* **118**, 3506–3518 (2013).
4. S. Horton, *Seismol. Res. Lett.* **83**, 250–260 (2012).
5. C. Frohlich, C. Hayward, B. Stump, E. Potter, *Bull. Seismol. Soc. Am.* **101**, 327–340 (2011).
6. A. H. Justinic, B. Stump, C. Hayward, C. Frohlich, *Bull. Seismol. Soc. Am.* **103**, 3083–3093 (2013).
7. C. Frohlich, *Proc. Natl. Acad. Sci. U.S.A.* **109**, 13934–13938 (2012).
8. A. McGarr, *J. Geophys. Res.* **119**, 1008–1019 (2014).
9. The Central and Eastern United States is considered the portion of the contiguous United States east of 109°W.
10. ANSS catalog, United States Geological Survey, http://earthquake.usgs.gov/earthquakes/search/, accessed 4/1/2014.
11. N. J. van der Elst, H. M. Savage, K. M. Keranen, G. A. Abers, *Science* **341**, 164–167 (2013).
12. D. F. Sumy, E. S. Cochran, K. M. Keranen, M. Wei, G. A. Abers, *J. Geophys. Res.* **119**, 1904–1923 (2014).
13. S. D. Davis, C. Frohlich, *Seismol. Res. Lett.* **64**, 207–224 (1993).
14. Information on materials and methods is available on *Science* Online.
15. Oklahoma Corporation Commission Imaging Web Application, http://imaging.occeweb.com/
16. D. Chernicky, *World Oil* (2000); www.worldoil.com/September-2000-Major-reserve-increase-obtained-by-dewatering-high-water-saturation-reservoirs.html.
17. K. E. Murray, *Environ. Sci. Technol.* **47**, 4918–4925 (2013).
18. F. Waldhauser, W. L. Ellsworth, *Bull. Seismol. Soc. Am.* **90**, 1353–1368 (2000).
19. A. A. Holland, *Seismol. Res. Lett.* **84**, 876–890 (2013).
20. D. L. Wells, K. J. Coppersmith, *Bull. Seismol. Soc. Am.* **84**, 974–1002 (1994).
21. P. A. Reasenberg, R. W. Simpson, *Science* **255**, 1687–1690 (1992).
22. L. Seeber, J. G. Armbruster, *Nature* **407**, 69–72 (2000).
23. R. Stein, *Nature* **402**, 605–609 (1999).
24. M. D. Zoback, J. Townend, B. Grollimund, *Int. Geol. Rev.* **44**, 383–401 (2002).
25. M. L. Zoback, *J. Geophys. Res.* **97**, 11703–11728 (1992).
26. K. V. Luza, J. E. Lawson, *Oklahoma Geological Survey Spec. Pub.* **81-3**, 1–67 (1981).
27. S. P. Gay, *Shale Shaker* **54**, 39–49 (2003).
28. L. E. Gatewood, in *Geology of Giant Petroleum Fields*, AAPG Memoir **14**, M. T. Halbouty, Ed. (American Association of Petroleum Geologists Tulsa, OK, 1970).
29. Monthly average volume was calculated by using reported volumes for any month with nonzero volume in data available from 1995 through 2012 (*15*). Injection rates over 90% larger than the median monthly value in a given year for each well were removed from calculations to remove data entry errors.

ACKNOWLEDGMENTS

This research benefited from discussion with E. Cochran, W. Ellsworth, and participants in a U.S. Geological Survey (USGS) Powell Center Working Group on Understanding Fluid Injection Induced Seismicity (M.W., B.A.B., and S.G. are part of this group). C. Hogan identified many *P* and *S* phases. K.M.K was partially supported by USGS National Earthquake Hazards Reduction Program (NEHRP) grant G13AP00025, M.W. was partially supported by the USGS Powell Center grant G13AC00023, and G.A.A. was partially supported by NEHRP grant G13AP00024. This project used seismic data from EarthScope's Transportable Array, a facility funded by the National Science Foundation. Seismic waveforms are from the Incorporated Research Institutions for Seismology Data Management Center and the USGS CWB Query. Well data are from the Oklahoma Corporation Commission and the Oklahoma Geological Survey. Lists of wells and the local earthquake catalog are available as supplementary materials on *Science* Online.

SUPPLEMENTARY MATERIALS

www.sciencemag.org/content/345/6195/448/suppl/DC1
Materials and Methods
Figs. S1 to S10
Tables S1 to S9
References (*30*–*41*)

8 May 2014; accepted 24 June 2014
Published online 3 July 2014;
10.1126/science.1255802

DINOSAUR EVOLUTION

A Jurassic ornithischian dinosaur from Siberia with both feathers and scales

Pascal Godefroit,[1]* Sofia M. Sinitsa,[2] Danielle Dhouailly,[3] Yuri L. Bolotsky,[4] Alexander V. Sizov,[5] Maria E. McNamara,[6,7] Michael J. Benton,[7] Paul Spagna[1]

Middle Jurassic to Early Cretaceous deposits from northeastern China have yielded varied theropod dinosaurs bearing feathers. Filamentous integumentary structures have also been described in ornithischian dinosaurs, but whether these filaments can be regarded as part of the evolutionary lineage toward feathers remains controversial. Here we describe a new basal neornithischian dinosaur from the Jurassic of Siberia with small scales around the distal hindlimb, larger imbricated scales around the tail, monofilaments around the head and the thorax, and more complex featherlike structures around the humerus, the femur, and the tibia. The discovery of these branched integumentary structures outside theropods suggests that featherlike structures coexisted with scales and were potentially widespread among the entire dinosaur clade; feathers may thus have been present in the earliest dinosaurs.

The origin of birds is one of the most-studied diversification events in the history of life. Principal debates relate to the origin of key avian features such as wings, feathers, and flight (*1*–*9*). Numerous finds from China have revealed that diverse theropods possessed feathers and various degrees of flight capability (*4*–*9*). The identification of melanosomes in non-avian theropods (*10*, *11*) confirms that fully birdlike feathers originated within Theropoda at least 50 million years before *Archaeopteryx*.

But were feathers more widespread among dinosaurs? Quill-like structures have been reported in the ornithischians *Psittacosaurus* (*12*) and *Tianyulong* (*13*), but whether these were true feathers, or some other epidermal appendage, is unclear. Bristlelike epidermal appendages occur in pterosaurs, some early theropods (*14*), and extant mammals ("hairs"), and so the *Psittacosaurus*

[1]Directorate 'Earth and History of Life,' Royal Belgian Institute of Natural Sciences, Rue Vautier 29, B-1000 Brussels, Belgium. [2]Institute of Natural Resources, Ecology and Cryology, 26 Butin Street, 672 014 Chita, Russia. [3]UJF-CNRS FRE 3405, AGIM, Université Joseph Fourier, Site Santé, 38 706 La Tronche, France. [4]Institute of Geology and Nature Management, FEB RAS, 1 Relochny Street 675 000, Blagoveschensk, Russia. [5]Institute of the Earth Crust, SB RAS, 128 Lermontov Street, Irkutsk, 664 033 Irkutsk, Russia. [6]School of Biological, Earth and Environmental Science, University College Cork, Cork, Ireland. [7]School of Earth Sciences, University of Bristol, Bristol BS8 1RJ, UK.
*Corresponding author. E-mail: pascal.godefroit@naturalsciences.be

body in sharks and a regionalized body with a pivoting neck joint and rigid trunk armor in arthrodires. Their evolutionary importance hinges on whether eubrachythoracid musculature is specialized or primitive relative to that of sharks. Placoderms appear to be a paraphyletic segment of the gnathostome stem group (*3*, *4*), so if any components of eubrachythoracid musculature can be shown to be general for placoderms, they can also be inferred to be primitive relative to the crown group. The status of the shallow myoseptal curvature cannot yet be determined in this regard, but the muscles of the neck joint and abdomen have specific skeletal associations that allow such phylogenetic inferences to be drawn.

Most ostracoderms, a grade of jawless stem gnathostomes (*2*) (Fig. 1A), have head shields that also encompass the shoulder-girdle region (*2*). This suggests that the gnathostome shoulder girdle originated through subdivision of the shield. Almost all placoderms have a mobile joint between the skull and shoulder girdle, implying the need for elevator and depressor muscles such as those observed in eubrachythoracids. Thus, a cucullaris operating this joint, antagonistic to specialized epaxial head elevators, is probably primitive relative to the crown gnathostome condition of a cucullaris without specialized antagonists that forms part of a broadly flexible neck.

The transverse abdominal muscles of eubrachythoracids are not as directly tied to a skeletal structure with an identifiable mechanical function. Comparison with those of a recent elephant shark indicates that these muscles are not homologous with any muscles of the pelvic fin or male clasper (supplementary text). However, the transverse abdominals may modulate shear forces between the armor and the laterally undulating body during tail-propelled swimming. A long ventral armor is also present in antiarchs, recovered as the most primitive placoderms in several recent analyses (*3*, *4*, *15*). Transverse abdominal muscles may thus be an attribute of the placoderm segment of the gnathostome stem group and, hence, primitive relative to the absence of such muscles at the base of the gnathostome crown group.

Outside of placoderms, transversely oriented abdominal muscle fibers are restricted to tetrapods and have been regarded as a tetrapod autapomorphy (*16*). Their associated connective tissues and tendons are derived from the somatopleure component of the lateral plate mesoderm (*17*), which plays an important role in hypaxial myogenesis (*18*). In lampreys, the posterior lateral plate mesoderm is not separated into splanchnic and somatopleuric components (*19*), meaning that it cannot give rise to somatopleure-derived structures such as paired fins. The presence of paired fins in placoderms shows that separation of somatopleure and splanchnopleure had occurred, supporting the inference that their transverse muscles may have been patterned by the same somatopleure-based mechanism as in tetrapods.

The arthodires of the Gogo Formation reveal an elaborate regionalized musculature, including the earliest and phylogenetically deepest examples of several muscle types. Particularly surprising is the extensive development of transverse-fiber muscles in the ventral body wall, which parallels the condition in tetrapods. Hypothetical reconstructions are not able to recover the full complexity of this musculature, either on the basis of biomechanical analysis or phylogenetic bracketing, and are thus liable to give a false picture of muscular evolution at the origin of gnathostomes. The study of exceptionally preserved fossils will continue to provide essential data for the reconstruction of vertebrate soft anatomy, particularly in groups with no close living relatives.

References and Notes

1. Y. Oisi, K. G. Ota, S. Kuraku, S. Fujimoto, S. Kuratani, *Nature* **493**, 175–180 (2013).
2. P. Janvier, *Early Vertebrates* (Clarendon Press, Oxford, 1996).
3. M. D. Brazeau, *Nature* **457**, 305–308 (2009).
4. S. P. Davis, J. A. Finarelli, M. I. Coates, *Nature* **486**, 247–250 (2012).
5. T. Matsuoka *et al*., *Nature* **436**, 347–355 (2005).
6. J. Mallatt, *Zool. J. Linn. Soc.* **117**, 329–404 (1996).
7. S. Kuratani, *J. Anat.* **205**, 335–347 (2004).
8. S. Kuratani, *Dev. Growth Differ.* **50** (suppl. 1), S189–S194 (2008).
9. A. Heintz, in *The Bashford Dean Memorial Volume: Archaic Fishes*, E. W. Gudger, Ed. (American Museum of Natural History, New York, 1930), pp. 115–224.
10. R. Miles, T. S. Westoll, *Trans. R. Soc. Edinb.* **67**, 373–476 (1968).
11. F. H. Edgeworth, *The Cranial Muscles of Vertebrates* (Cambridge Univ. Press, Cambridge, 1935).
12. K. Trinajstic, C. Marshall, J. Long, K. Bifield, *Biol. Lett.* **3**, 197–200 (2007).
13. S. Gemballa *et al*., *Proc. Biol. Sci.* **270**, 1229–1235 (2003).
14. S. A. Wainwright, F. Vosburgh, J. H. Hebrank, *Science* **202**, 747–749 (1978).
15. M. Zhu, X. Yu, B. Choo, J. Wang, L. Jia, *Biol. Lett.* **8**, 453–456 (2012).
16. N. Schilling, *Front. Zool.* **8**, 4 (2011).
17. B. Christ, M. Jacob, H. J. Jacob, *Anat. Embryol.* **166**, 87–101 (1983).
18. S. J. Mathew *et al*., *Development* **138**, 371–384 (2011).
19. K. Onimaru, E. Shoguchi, S. Kuratani, M. Tanaka, *Dev. Biol.* **359**, 124–136 (2011).

Acknowledgments: We acknowledge M. Siversson at the Western Australian Museum, Perth, and Z. Johanson at the Natural History Museum, London, for lending us specimens in their care. We thank I. Montero Verdú for his picture of the muscle bundles (Fig. 3D) and A. Ritchie for an *Eastmanosteus* image. K.T., P.E.A., and C.B. are supported by Australian Research Council (ARC) QEII Fellowship DP 110101127; J.L., K.T., T.S., and G.Y. by ARC DP 1092870; S.S., V.D., and P.E.A. by European Research Council Advanced Investigator Grant 233111; P.E.A. by a Wallenberg Scholarship from the Knut and Alice Wallenberg Foundation; and C.B. by a Human Frontiers Research Program and an ARC Discovery Project, DP 1096002. The scan performed at the European Synchrotron Radiation Facility in Grenoble, France, was part of project EC770. K.T. acknowledges the 2010 Prime Minister's Science Prize, and J.L. acknowledges funding from The Australian Geographic Society, which supported fieldwork at the Gogo Formation. Specimens are housed in the collections of the Western Australian Museum, Australian National University, Australian Museum, and Museum Victoria, Australia, and the Natural History Museum, UK.

Supplementary Materials

www.sciencemag.org/cgi/content/full/science.1237275/DC1
Materials and Methods
Supplementary Text
Figs. S1 to S4
References (*20*–*30*)
Movie S1

4 March 2013; accepted 29 May 2013
Published online 13 June 2013;
10.1126/science.1237275

Enhanced Remote Earthquake Triggering at Fluid-Injection Sites in the Midwestern United States

Nicholas J. van der Elst,[1]* Heather M. Savage,[1] Katie M. Keranen,[2]† Geoffrey A. Abers[1]

A recent dramatic increase in seismicity in the midwestern United States may be related to increases in deep wastewater injection. Here, we demonstrate that areas with suspected anthropogenic earthquakes are also more susceptible to earthquake-triggering from natural transient stresses generated by the seismic waves of large remote earthquakes. Enhanced triggering susceptibility suggests the presence of critically loaded faults and potentially high fluid pressures. Sensitivity to remote triggering is most clearly seen in sites with a long delay between the start of injection and the onset of seismicity and in regions that went on to host moderate magnitude earthquakes within 6 to 20 months. Triggering in induced seismic zones could therefore be an indicator that fluid injection has brought the fault system to a critical state.

Earthquakes can be induced by underground fluid injection, which increases pore pressure and allows faults to slide under preexisting shear stress (*1*). The increase in wastewater disposal from natural gas development and other sources has been accompanied by an increase in fluid-induced earthquakes in recent years (*2*). These earthquakes include widely felt earthquakes in

Oklahoma, Arkansas, Ohio, Texas, and Colorado (Fig. 1) (*3*–*7*). Although most injection wells are not associated with large earthquakes, the converse is not true. At least half of the 4.5 moment magnitude (M_w) or larger earthquakes to strike the interior of the United States in the past decade have occurred in regions of potential injection-induced seismicity (table S1). In some cases, the onset of seismicity follows injection by only days or weeks (*1*, *3*, *5*), and the association with pumping at particular wells is clear. In others, seismicity increases only after months or years of active injection (*4*, *8*, *9*).

A long delay before seismic activation implies that faults may be moving toward a critical state for years before failure. However, currently there are no reliable methods to determine whether a particular field has reached a critical state other than by simply observing a large increase in seismicity. This lack of diagnostics is a key problem in developing operational strategies to mitigate anthropogenic activity (*2*).

Because induced seismic zones are brought to failure by increased pore pressures, we examined whether areas of induced seismicity show a high susceptibility to dynamic triggering by the small transient stresses carried by seismic waves from distant earthquakes. Dynamic triggering in natural settings has been linked to the presence of subsurface fluids, and seismicity rate changes have been shown to depend systematically on the perturbation stress (*10*–*13*). This suggests that dynamic triggering could serve as a probe of the state of stress in areas of wastewater injection. We refer to earthquakes that are promoted by anthropogenic activity as induced and to earthquakes that are initiated by transient natural stresses as triggered. By this definition, there can be triggered induced earthquakes.

A search of the Advanced National Seismic System (ANSS) earthquake catalog gives preliminary evidence that induced seismic zones are sensitive to dynamic triggering by surface waves (Fig. 1). Regions of suspected induced seismicity showed a pronounced increase in 3.0 M and larger earthquakes spanning at least a 3-day window after large ($M_w \geq 8.6$) remote earthquakes: the 27 February 2010 8.8 M_w Maule, Chile; 11 March 2011 9.1 M_w Tohoku-oki; and 12 April 2012 8.6 M_w Sumatra earthquakes. The broader central United States shows essentially no response to these events (Fig. 1). Most of the triggering is at three sites: Prague, Oklahoma; Snyder, Texas; and Trinidad, Colorado. Suggestively, each of these regions went on to host moderate to large earthquakes (4.3 to 5.7 M_w) within 6 to 20 months of the strong triggering.

Although the triggering is significant at the 96% level (table S2), a closer investigation is warranted. We therefore enhanced the catalog by applying a single-station matched filter to continuous waveforms (*14*). The matched-filter approach identifies small, uncataloged earthquakes based on their similarity to target events (*15*–*17*). Distinct families of earthquakes are distinguished based on the difference in P and S wave travel times (S-P time), which gives the approximate radial distance from the seismic station (*15*).

The Cogdell oil field (*8*), located near Snyder, Texas, hosted a seismic swarm in September 2011 that included a 4.3 M_w main shock (supplementary text). The enhanced catalog shows that the Tohoku-oki earthquake triggered a significant number of earthquakes (*14*) at this site (Fig. 2 and table S2). In fact, the rate of earthquakes within the 10 days after the Tohoku-oki earthquake was the highest observed over the entire study duration (February 2009 to present), excluding the days immediately after the 4.3 M_w main shock. The triggered earthquakes show a swarm like signature, typical of fluid-induced earthquakes (*18*), with the largest of the triggered events (3.8 M_w, ANSS) occurring after 2.5 days of smaller events (Fig. 2C). The much earlier February 2010 Maule earthquake did not trigger at Snyder, nor did the post-swarm April 2012 Sumatra earthquake.

Prague, Oklahoma, experienced three 5.0 M_w and greater earthquakes in November 2011, associated with fluid disposal in the Wilzetta field (supplementary text) (*4*). The enhanced catalog shows that the February 2010 Maule event triggered a strong sequence of earthquakes near the eventual epicenter of the first 5.0 M_w earthquake (Fig. 3 and table S2). The rate of earthquakes in the several days after the Maule trigger far exceeds that of any other time within the period of observation, up to the $M_w \geq 5.0$ earthquakes themselves, which is similar to the observation at Snyder. There are no events detected within ±32 km relative distance for at least 4 months before the 2010 Maule earthquake.

The largest event in the remotely triggered sequence is a 4.1 M_w, 16 hours after the 2010 Maule earthquake, which may account for the large number of earthquakes that continued up to the time of the first 5 M_w Prague earthquake in 2011 (Fig. 3). If the 4.1 M_w earthquake can be considered a foreshock of the subsequent 5.7 M_w Prague earthquake, then the 5.7 M_w event is not only one of the largest earthquakes to be associated with wastewater disposal (*2*) but also one of the largest earthquakes to be linked indirectly to a remote triggering event (*4*, *19*).

The April 2011 Tohoku-oki earthquake, which occurred during the ongoing sequence before the 5.7 M_w Prague main shock, did not trigger additional earthquakes near the swarm (Fig. 3 and table S2). The 2012 Sumatra earthquake, on the other hand, followed the main 5.7 M_w Prague earthquake by 5 months and triggered a small uptick in activity that was consistent with the far northeastern tip of the swarm (Fig. 3C). However, this triggered rate change is much smaller than that triggered by the Maule earthquake in 2010.

Trinidad, Colorado, experienced a seismic swarm in August 2011 that included a 5.3 M_w main shock, possibly related to coal-bed methane extraction and reinjection of the produced water in the Raton Basin (supplementary text). The February 2010 Maule earthquake triggered a small but statistically significant response near the site of the 5.3 M_w main shock (Fig. 4 and table S2). Although the total number of triggered events is small (four), the binomial probability of observ-

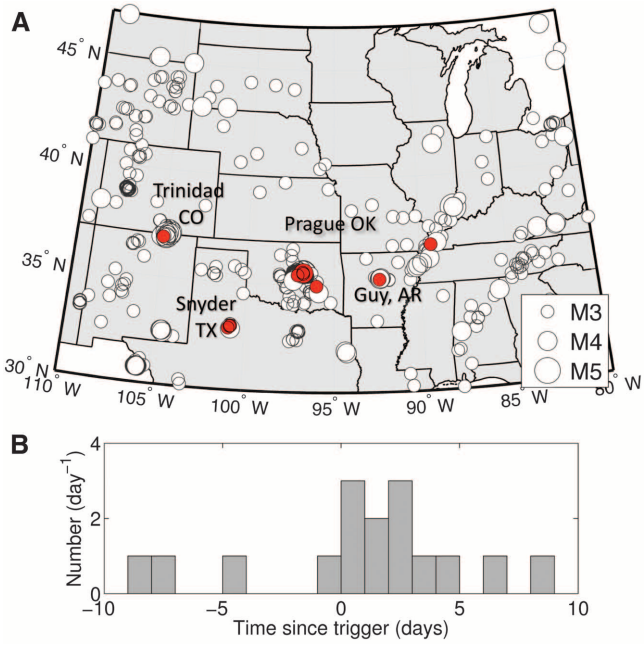

Fig. 1. Remote triggering in the midwestern United States, from the composite ANSS catalog. (**A**) Cataloged earthquakes above 3.0 M between 2003 and 2013 (ANSS). Earthquakes in red occurred during the first 10 days after the February 2010, Maule; March 2011, Tohoku-oki; or April 2012, Sumatra earthquakes. Triggering occurs almost exclusively in three injection fields, labeled Prague, Trinidad, and Snyder. (**B**) Stacked earthquake counts in the 10 days before and after the three ≥8.6 M_w remote earthquakes. The histogram excludes the Guy, Arkansas, swarm, which dominates event rates at the time of the 2011 Tohoku-oki earthquake but did not trigger (supplementary text).

[1]Lamont-Doherty Earth Observatory of Columbia University, Post Office Box 1000, 61 Route 9W, Palisades, NY 10964, USA. [2]ConocoPhillips School of Geology and Geophysics, University of Oklahoma, 100 East Boyd Street, Norman, OK 73069, USA.

*Corresponding author. E-mail: nicholas@ldeo.columbia.edu
†Present address: Department of Earth and Atmospheric Sciences, Cornell University, 410 Thurston Avenue, Ithaca, NY 14850, USA.

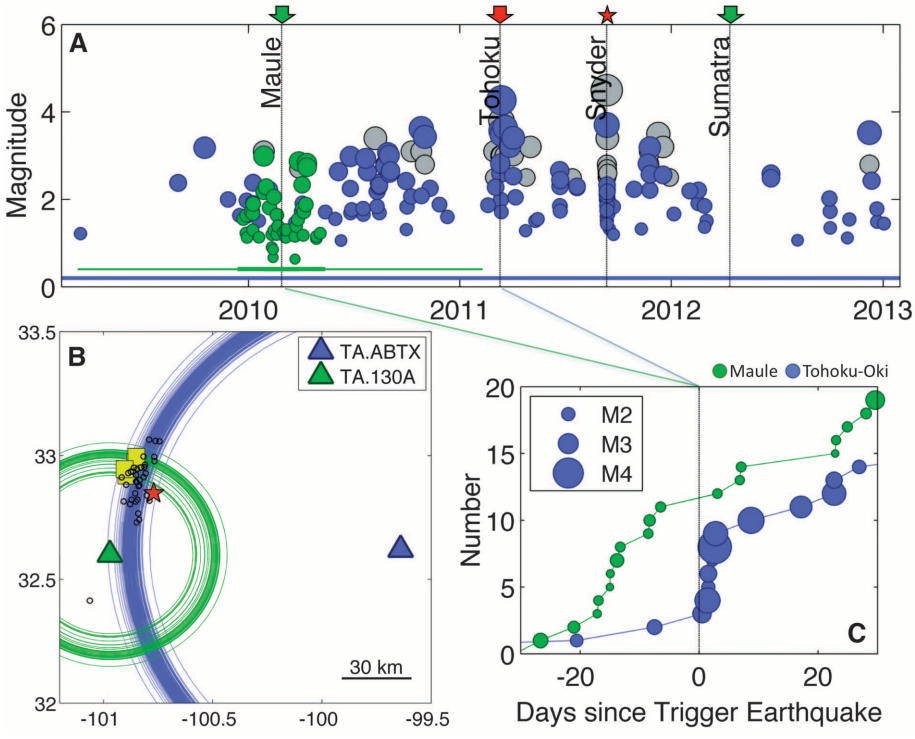

Fig. 2. Matched-filter enhanced catalog for Snyder, Texas. (**A**) Detected events, showing triggering by the 2011 Tohoku-oki earthquake. Symbols along top show strength of triggering (red, strong; green, none). Red star marks 11 September 2011 4.3 M_w main shock (NEIC catalog). Colors correspond to station in (B), with ANSS catalog in gray. Seismometer operating times and the times at which we have enhanced the catalog are shown by thin and thick horizontal bars, respectively. (**B**) Mapped distances to detected events. Small circles are ANSS catalog earthquakes; a red star shows the main shock. Yellow squares are nearby active injection wells. (**C**) Cumulative event count around the 2010 Maule and 2011 Tohoku-oki earthquakes.

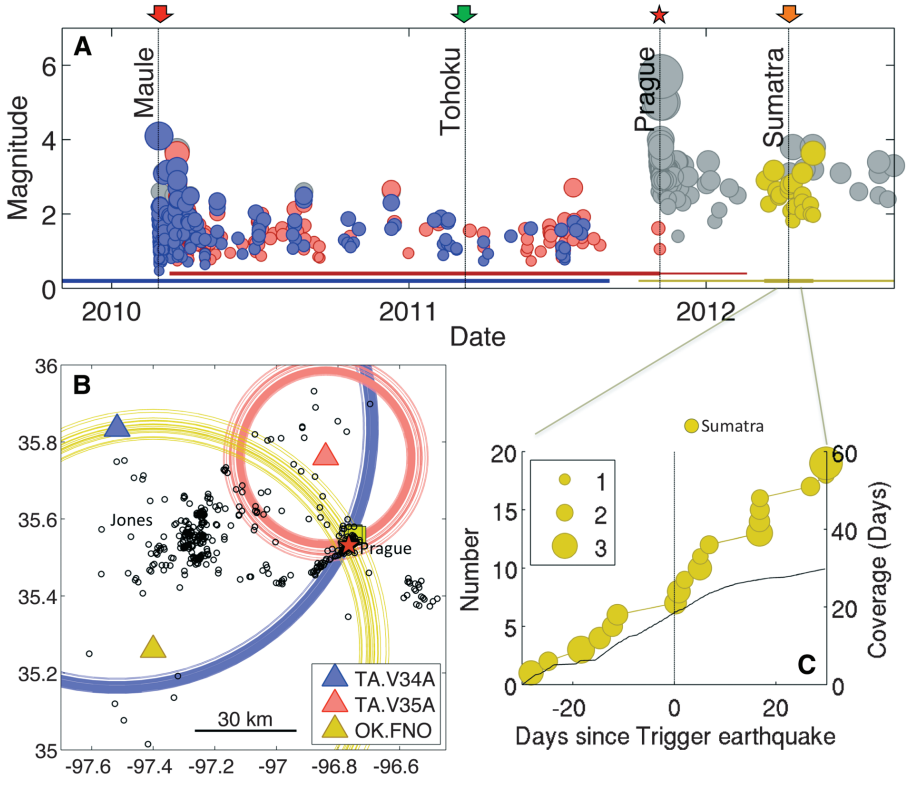

Fig. 3. Matched-filter enhanced catalog for Prague, Oklahoma. (**A**) Detected events, showing triggering by the 2010 Maule earthquake. Red star marks the 6 November 2011 5.7 M_w main shock. Other details are as in Fig. 2A. (**B**) Mapped distances to detected events. Details are as in Fig. 2B. (**C**) Cumulative event count around the 2012 Sumatra earthquake. Cumulative recording time for this intermittently operating station is shown over the same period.

ing this many events in 1 day after the trigger, given five events in the entire previous year, is less than 10^{-5}.

The March 2011 Tohoku-oki earthquake, which occurred during the active portion of the swarm, did not trigger additional seismicity at Trinidad. The 2012 Sumatra earthquake occurred 8 months after the 5.3 M_w Trinidad main shock and triggered a moderate surge in activity that was consistent with the far edge of the swarm, where previous swarm activity had not occurred (fig. S2). This pattern—strong triggering by the first remote earthquake, none by the second, and marginal triggering after the swarm—is very similar to that observed in Oklahoma.

We examined several other regions in the United States that have experienced moderate magnitude earthquakes or heightened seismicity rates linked to fluid injection, including Guy, Arkansas; Jones, Oklahoma; and Youngstown, Ohio. None of these other regions appear to have responded to remote triggering (supplementary text).

The strongly triggered regions were exceptional in that they had a long history of pumping within 10 km of the eventual swarms yet were relatively quiet for much of that history. At other sites of induced moderate earthquakes (Guy, Arkansas, and Youngstown, Ohio), the lag time between the start of pumping and onset of seismicity was as little as months or weeks, presenting a relatively small window of vulnerability to dynamic triggering before the swarms.

The delay in induced seismicity in some regions could be due to complexities in the local geology (supplementary text). In Oklahoma, injection occurred into a fault-bounded pocket, and pressures may have built up slowly over time because of the size of the reservoir bounded by impermeable faults (*4*). The Cogdell field may have similar isolated pockets, formed by discrete carbonate reefs buried within impermeable shales (*8*).

Fluids have been suggested as an important component in dynamic triggering since early

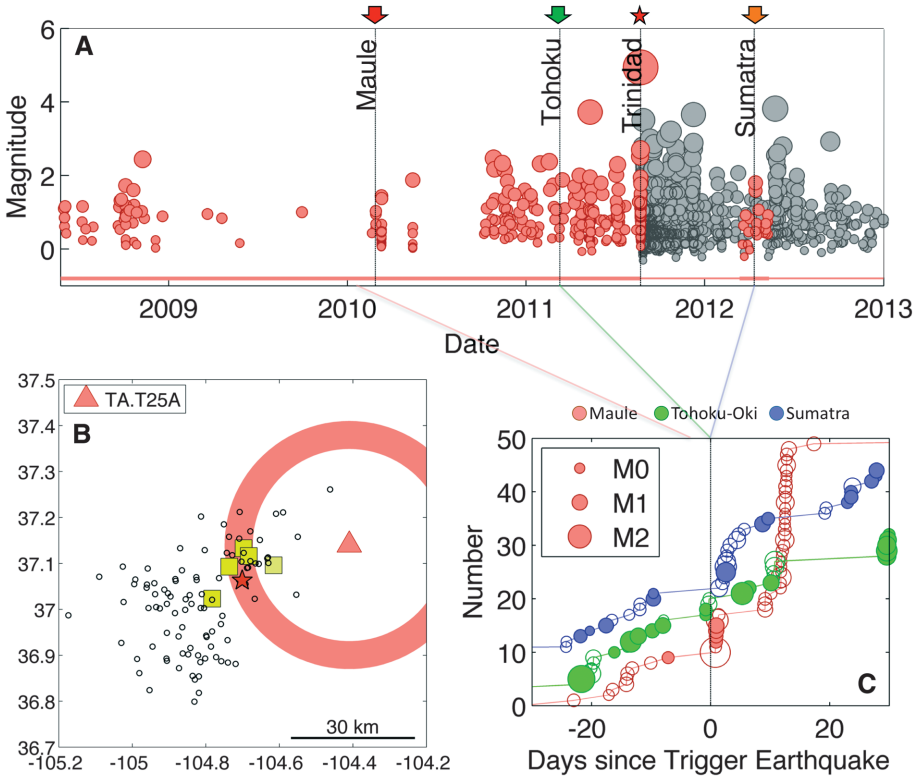

Fig. 4. Matched-filter enhanced catalog for Trinidad, Colorado. (**A**) Detected events, showing triggering by the 2010 Maule earthquake. Red star marks the 23 August 2011 5.3 M_w main shock. Other details are as in Fig. 2A. (**B**) Mapped distances to detected events. Details are as in Fig. 2B. (**C**) Waveform detection counts around the 2010 Maule, 2011 Tohoku-oki, and 2012 Sumatra earthquakes (curves offset for clarity). Filled circles are within 2.5-km radial distance relative to the 5.3 M_w main shock, and open circles are within ~5 km (fig. S2).

observations showed preferential triggering in active volcanic and hydrothermal systems (*13*, *20*, *21*). Some features of our observations are also suggestive of a fluid mechanism for triggering. First, in all of the studied cases the triggered earthquakes occurred with a small delay with respect to the passage of the seismic waves, initiating within less than 24 hours and continuing for days to months afterward. This pattern suggests a triggering mechanism that relies on dynamic permeability enhancement and transport of fluids (*22*, *23*), as has been suggested for natural triggered seismicity (*20*–*22*). In this scenario, stress transients alter the permeability of hydraulic conduits in the reservoir, accelerating diffusion of pore pressure into local faults. Fractures in active injection reservoirs may be particularly susceptible to this mechanism because the injection of unequilibrated fluids may lead to clogging through mineralization and sedimentation. A brief pressure transient may then flush out these clogged fractures (*22*, *24*).

In Prague and Trinidad, only the first of two large remote events caused earthquakes, despite imparting dilational and shear strains that are similar to subsequent events (table S4). This is also consistent with the permeability enhancement model, which requires a certain amount of recharge time between triggering episodes (*24*). After local fault slip is triggered, the local permeability rises dramatically because of microfracturing and dilation (*25*), promoting further fluid diffusion over several rupture dimensions (*26*). Hence, once the seismic swarm is underway the fractures may not return to a state in which they are susceptible to unclogging by small transient stresses.

We find that certain areas of fluid injection are sensitive to small changes in stress associated with the passage of seismic waves from remote large earthquakes. The observations suggest several requirements for an induced region to be sensitive to remote triggering. First, all of the triggered sites in this study had a long history of regional subsurface injection over a period of decades. Second, each triggered site was near to hosting a moderate magnitude earthquake, suggesting critically stressed faults. Last, each site had relatively low levels of seismicity rate in the immediate vicinity (10 km) before the first triggering episode. Remote triggering can therefore indicate that conditions within an injection field have crossed some critical threshold, and a larger induced earthquake could be possible or even likely. This underlines the importance of improved seismic monitoring in areas of subsurface fluid injection.

References and Notes

1. C. B. Raleigh, J. H. Healy, J. D. Bredehoeft, *Science* **191**, 1230–1237 (1976).
2. National Research Council, *Induced Seismicity Potential in Energy Technologies* (National Academies Press, New York, 2012).
3. S. Horton, *Seismol. Res. Lett.* **83**, 250–260 (2012).
4. K. M. Keranen, H. M. Savage, G. A. Abers, E. S. Cochran, *Geology* **41**, 699–702 (2013).
5. W.-Y. Kim, "Induced seismicity associated with fluid injection into deep wells in Youngstown, Ohio," abstract S43D-2496 presented at 2012 Fall Meeting, American Geophysical Union, San Francisco, CA, 3 to 7 December 2012.
6. C. Frohlich, J. Glidewell, M. Brunt, *Bull. Seismol. Soc. Am.* **102**, 457–466 (2012).
7. J. L. Rubinstein, W. L. Ellsworth, A. McGarr, "The 2001–present triggered seismicity sequence in the Raton basin of southern Colorado/Northern New Mexico," BSSA Abstracts 2013 Annual Meeting 155D, (2013).
8. S. D. Davis, W. D. Pennington, *Bull. Seismol. Soc. Am.* **79**, 1477–1494 (1989).
9. R. B. Horner, J. E. Barclay, J. M. MacRae, *Can. J. Explor. Geophys.* **30**, 39–50 (1994).
10. N. J. van der Elst, E. E. Brodsky, *J. Geophys. Res.* **115**, B07311 (2010).
11. H. M. Savage, C. Marone, *J. Geophys. Res.* **113**, B05302 (2008).
12. D. P. Hill, S. G. Prejean, in *Dynamic Triggering*, vol. 4, H. Kanamori, Ed., Treatise on (Elsevier, New York, 2007), pp. 257 to 292.
13. D. P. Hill *et al.*, *Science* **260**, 1617–1623 (1993).
14. Materials and methods are available as supplementary materials on *Science* Online.
15. C. Frohlich, C. Hayward, B. Stump, E. Potter, *Bull. Seismol. Soc. Am.* **101**, 327–340 (2011).
16. Z. G. Peng, P. Zhao, *Nat. Geosci.* **2**, 877–881 (2009).
17. D. R. Shelly, G. C. Beroza, S. Ide, *Nature* **446**, 305–307 (2007).
18. J. E. Vidale, P. M. Shearer, *J. Geophys. Res.* **111**, B05312 (2006).
19. T. Parsons, A. A. Velasco, *Nat. Geosci.* **4**, 312–316 (2011).
20. E. E. Brodsky, S. G. Prejean, *J. Geophys. Res.* **110**, B04302 (2005).
21. S. Husen, R. Taylor, R. B. Smith, H. Healser, *Geology* **32**, 537–540 (2004).
22. E. E. Brodsky, E. Roeloffs, D. Woodcock, I. Gall, M. Manga, *J. Geophys. Res.* **108**, (B8), 2390 (2003).
23. T. Taira, P. G. Silver, F. L. Niu, R. M. Nadeau, *Nature* **461**, 636–639 (2009).
24. J. E. Elkhoury, A. Niemeijer, E. E. Brodsky, C. Marone, *J. Geophys. Res.* **116**, (B2), B02311 (2011).
25. T. M. Mitchell, D. R. Faulkner, *J. Geophys. Res.* **113**, (B11), B11412 (2008).
26. S. Micklethwaite, S. F. Cox, *Earth Planet. Sci. Lett.* **250**, 318–330 (2006).

Acknowledgments: This paper benefitted from discussions with E. Brodsky and W.-Y. Kim. Injection data for Cogdell Oilfield was provided by C. Frohlich. The Oklahoma Corporation Commission, the Texas Railroad Commission, and the Colorado Oil and Gas Conservation Commission supplied well databases. Earthquake locations were provided by ANSS. Seismic waveforms are from the Incorporated Research Institutions for Seismology Data Management Center. N.J.v.d.E. was supported by U.S. National Science Foundation (NSF) grant EAR-1144503. H.M.S. and G.A.A. were partially supported by U.S. Geological Survey (USGS) National Earthquake Hazards Reduction Program (NEHRP) grant G13AP00024. K.M.K. received support from USGS NEHRP grant G13AP00025. This project made use of EarthScope's Transportable Array, a facility funded by NSF. The enhanced seismicity catalogs are available as supplementary materials on *Science* Online.

Supplementary Materials

www.sciencemag.org/cgi/content/full/341/6142/164/DC1
Materials and Methods
Supplementary Text
Figs. S1 to S5
Tables S1 to S5
References (*27*–*43*)
Database S1

9 April 2013; accepted 23 May 2013
10.1126/science.1238948